

Article

Growth of Sesquioxide Crystals from Tungsten Crucibles by Vertical Gradient Freezing Method

Evgeny Galenin ¹, Viktoriia Galenina ¹, Iaroslav Gerasymov ¹, Daniil Kurtsev ¹, Serhii Tkachenko ¹, Pavlo Arhipov ¹, Sofiia Sadivnycha ^{1,2}, Vadim Alekseev ¹, Anna Shaposhnyk ³, Ianina Boiaryntseva ¹, Vira Niestierkina ^{1,4}, Sandra Witkiewicz-Łukaszek ⁵, Yuriy Zorenko ⁵ and Oleg Sidletskiy ^{1,2,*}

¹ Institute for Scintillation Materials NAS of Ukraine, 60, Nauky Ave., 61072 Kharkiv, Ukraine

² Centre of Excellence ENSEMBLE3 Sp. Z O.O. ul, Wolczynska 133, 01-919 Warsaw, Poland

³ SSI "Institute for Single Crystals" NAS of Ukraine, 60, Nauky Ave., 61072 Kharkiv, Ukraine

⁴ Erwin Schrödinger International Institute for Mathematics and Physics, University of Vienna, Boltzmannngasse 9, 1090 Vienna, Austria

⁵ Department of Physics, Kazimierz Wielki University in Bydgoszcz, Powstancow Wielkopolskich Str., 2, 85-090 Bydgoszcz, Poland

* Correspondence: sidletskiy@isma.kharkov.ua or oleg.sidletskiy@ensemble3.eu

Abstract: Sesquioxides of lanthanides, yttrium, and scandium are promising hosts for laser and scintillation materials; however, the crystallization of such compounds is complicated by very high melting temperatures, as well as polymorph transitions. This work reports for the first time the growth of Y_2O_3 and $Y_{2-x}Sc_xO_3$ crystals by the Vertical Gradient Freezing method from tungsten crucibles, proposing an alternative to extremely expensive rhenium and iridium crucibles. Translucent Y_2O_3 samples are obtained, and their luminescent and scintillation parameters are evaluated. The main issues of Y_2O_3 crystallization under the proposed conditions are discussed, as well as ways of enhancing the crystal quality. Finally, polymorph transitions are avoided by decreasing the average radius of the rare earth cation by Y^{3+}/Sc^{3+} substitution, providing transparent $Y_{2-x}Sc_xO_3$ crystals with a cubic structure.



Citation: Galenin, E.; Galenina, V.; Gerasymov, I.; Kurtsev, D.; Tkachenko, S.; Arhipov, P.; Sadivnycha, S.; Alekseev, V.; Shaposhnyk, A.; Boiaryntseva, I.; et al. Growth of Sesquioxide Crystals from Tungsten Crucibles by Vertical Gradient Freezing Method. *Crystals* **2023**, *13*, 591. <https://doi.org/10.3390/cryst13040591>

Academic Editor: Xiang-Hua Zhang

Received: 28 February 2023

Revised: 23 March 2023

Accepted: 27 March 2023

Published: 31 March 2023



Copyright: © 2023 by the authors. Licensee MDPI, Basel, Switzerland. This article is an open access article distributed under the terms and conditions of the Creative Commons Attribution (CC BY) license (<https://creativecommons.org/licenses/by/4.0/>).

Keywords: crystal growth; sesquioxides; vertical gradient freezing; scintillator; carbidization; tungsten crucible

1. Introduction

Sesquioxides are attractive hosts for applications in optics, lasers, and scintillators. In particular, a fast scintillation response was reported in undoped Y_2O_3 and Sc_2O_3 [1], while Y_2O_3 and Lu_2O_3 doped with other rare earths were proposed as alpha detectors and luminophores [2–4], as well as laser elements for technical and medical applications [5,6]. In particular, the reported light yields of Sc_2O_3 , Y_2O_3 , and Lu_2O_3 were 16,200, 2600, and 200 ph/5.5 MeV-alpha, respectively. Under ^{137}Cs gamma-ray excitation, the light yields of Sc_2O_3 , Y_2O_3 , and Lu_2O_3 were 11,500, 3200, and 500 ph/MeV, respectively [1]. The scintillation decay times of these sesquioxides comprised several tens of nanoseconds [1]. Therefore, sesquioxides of lanthanides, scandium, and yttrium possess low-to-moderate light yield and fast scintillation decay. These properties in combination with an extremely high density of up to 9.42 g/cm^3 and effective atomic number of 68.8 in Lu_2O_3 [6] should provide an efficient registration of ionizing particles.

Lanthanide, scandium, and yttrium sesquioxides are compounds with extremely high melting temperatures of up to 2500 °C [7,8]. The technologies of their crystallization are complicated and energy consuming. Furthermore, a very limited range of materials may be used as crucibles for the crystallization of these compounds from melts. Some of the alternatives are a ceramic synthesis at temperatures well below the melting point [5,6,9–13], spark plasma sintering [1,14], and sol-gel synthesis [4]. Meanwhile, sesquioxide crystals

can be obtained by direct crystallization from melts by crucible-free methods, such as laser heating pedestal growth [14], or from rhenium crucibles by micro pulling down, edge-defined film-fed growth [15–18]; however, crystal size is limited in these methods to a few millimeters in the cross-section. The largest ingots of up to 40 mm in diameter and 30 mm in length were obtained by the HEM method [19,20], but crystals stuck to crucibles after the growth process, thus increasing the risk of destruction of crystals and expensive crucibles.

Recent works [21,22] reported a successful growth of mixed of Y and Sc sesquioxides by the Czochralski method. Y^{3+}/Sc^{3+} substitution decreases the averaged cationic radius in the composition, as well as reduces the crystallization temperature down to 2150 °C, making possible the usage of Ir crucibles. Furthermore, unlike in Y_2O_3 , there are no polymorph transitions between H-, B(monoclinic)-, and C (cubic) phases in $Y_{2-x}Sc_xO_3$ at a large enough x that ensures a direct crystallization by the Czochralski and other methods of growth from the melt. However, currently iridium is even more expensive than rhenium, and the lifetime of Ir crucibles at such temperatures is short, making this approach not economically feasible. At the same time, cheap tungsten crucibles with a melting temperature of ~3400 °C are also potentially applicable for the crystallization of sesquioxides from melts. For instance, $Sc_2O_3:Pr, Ho$ was crystallized from W crucibles in [23], but no details of the process were provided. Following our experience [24–26], high-melting-point oxide crystals may be grown from W crucibles under reducing atmosphere conditions, but the process is complicated by tungsten oxidation and its interaction with melts.

This work explores possibilities of using W crucibles for the crystallization of sesquioxides on the example of Y_2O_3 and mixed $Y_{2-x}Sc_xO_3$. The Vertical Gradient Freezing (VGF) method was chosen due to the possibility of protecting the melt from interaction with the reducing atmosphere in the growth chamber and good thermal insulation of the crystallizer in the absence of crystal/crucible pulling and any moving parts. Furthermore, this method should be scalable relatively easily. We report the methods to prevent the melt from interaction with the growth atmosphere and carbidization during the process of crystal growth, as well as structure, optical, and scintillation properties of the obtained crystals.

2. Materials and Methods

Powder of Y_2O_3 99.999% (Nexconn, Shenzhen, China) and Sc_2O_3 99.99% (Stanford Materials, Lake Forest, CA, USA) were used as starting materials. Bulk densities of raw material powders were around thrice lower as compared to single crystals. The powders were pressed into an Mo tube and sintered at temperatures from 1500 to 2250 °C to ensure the density of >95% with respect to the Y_2O_3 crystal. The largest density of >95% was achieved when the calcination temperature was increased up to 2250 °C. The sintered rods were then loaded into tungsten growth crucibles, which comprised tungsten rods of 10 mm in diameter with axially drilled holes of 6–9 mm in diameter. The crucibles of 20–40 mm height were installed inside the radiofrequency-heated (8 kHz) graphite insulation. Temperature was controlled with a WRe-thermocouple and a Raytek Marathon MM2MH pyrometer.

Crystals were grown by the VGF method with radiofrequency-heated graphite heaters and gradual cooling of the crucible starting from its bottom. The grown crystals were heat treated in air using a standard tube furnace at 1200 °C during a 12 h period. The heating/cooling rate was 200 °C/h. Then, plates of different thicknesses were fabricated for tests of luminescent and scintillation performance.

The powder diffraction measurements were carried out by Siemens D500 diffractometer, $CuK\alpha$ radiation, Bragg–Brentano geometry, curved graphite monochromator on the counter arm, $5 < 2\theta < 100^\circ$, and $\Delta 2\theta = 0.02^\circ$. The phases were identified using JCPDS PDF-1 card files and EVA retrieval system included in the diffractometer software.

Optical absorption spectra were measured using a Specord40 spectrophotometer operating in the 190–1100 nm wavelength range (Analytik Jena AG, Jena, Germany).

X-ray luminescence spectra were measured in the reflection mode under a steady-state X-ray excitation (Ag anode, 40 kV, 40 μ A). The emitted light was dispersed by a monochromator with 1200 grooves/mm grating and registered by the PMT Hamamatsu R1926A. The obtained spectra were not corrected for the spectral sensitivity of the detection system. Cathodoluminescence (CL) spectra were registered at RT using an e-beam in a SEM JEOL JSM-820 electron microscope equipped with a Stellar Net spectrometer and a TE-cooled CCD detector working in the 200–925 nm range. The light yield of CL was evaluated in comparison with etalon of Bi₄Ge₃O₁₂ (BGO) scintillator. BGO is used quite often as a reference for determination of light yield in scintillators, because this crystal possesses around the same light yield of around 8000–9000 phot/MeV independent of the producer [27]. The etalon used in the present work was produced at the Institute for Scintillation Materials NAS of Ukraine and possesses a light yield of 8600 phot/MeV [28].

Luminescence decay times were determined under γ -rays (¹³⁷Cs), α -particles (²³⁹Pu), and β -particles (²⁰⁷Bi). Scintillation pulses were registered by Hamamatsu R1307 PMT, the signal of which was transferred to Rigol DC1302CA digital oscillograph used as analog–digital converter. The obtained data were acquired by PC; 10,000 pulses were registered in each case.

All the measurements were conducted at room temperature (25 °C).

3. Results and Discussion

3.1. Preventing Melt from Carbidization

The crystal growth atmosphere of Ar+CO was formed by the interaction of residual oxygen in the growth chamber with the graphite heater and heat insulation at high temperatures by Reaction (1) proceeding at temperatures over 950 °C [29]:



Carbon dioxide may reduce or carbidize the Y₂O₃ melt by Reactions (2)–(4) [30]:



The extent of the negative influence of these reactions on Y₂O₃ melt purity was evaluated. The crucible was loaded with raw material, heated until melting, held for 24 h, and slowly cooled to room temperature. A phase analysis of the resulting material without any additional treatment was performed (Figure 1a). The XRD data indicate that the main phase was cubic Y₂O₃ (JCPDS 25-1200, Sp.gr. *Ia-3*, *a* = 10.607 Å), whereas remarkable quantities of metallic yttrium (JCPDS 12-0702, Sp.gr. *P6₃/mmc*, *a* = 3.647, *c* = 5.730) and yttrium oxycarbide YO_{0.7}C_{0.3} (JCPDS 38-1114, Sp.gr. *Fm3m*, *a* = 4.930) were detected as well (Figure 1b).

Then, the crucible was covered with a W lid and a set of protective W screens was installed to reduce gas diffusion between the graphite and melt and minimize the melt's interaction with carbon oxide. As the result, the contents of the YO_{0.7}C_{0.3} admixture phase and metallic yttrium were reduced (Figure 1b).

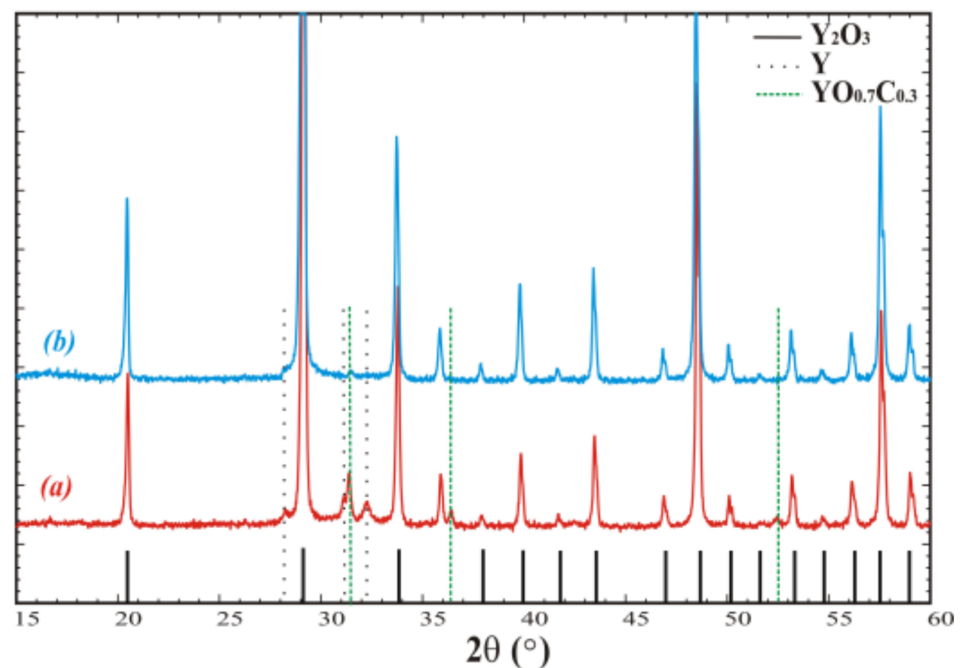


Figure 1. Powder diffraction patterns of crystallized Y_2O_3 (a) in open crucible and (b) in crucible covered with lid and additional screening. Peaks corresponding to the admixtures are denoted by the dashed and dotted vertical lines.

3.2. VFG Growth

The VGF method was chosen for crystal growth, as it does not require crucible/crystal translation and ensures better heat insulation, which is of special importance at very high temperatures. The thermal assembly design provided axial temperature distribution, illustrated in Figure 2. The crucible with raw material was installed so that its bottom corresponds to 0 mm in Figure 2. The graphite heaters were arranged in such a way to create a higher temperature in the upper part of the crucible as compared to the lower part, providing crystallization from the bottom upwards when decreasing the heating power. For example, for a crucible of 50 mm length, the temperature difference between the top and bottom was 60 °C. As the crystallization process was not controlled visually, the power regimes were adjusted by observing the melting of Y_2O_3 etalons located at the top and bottom of the crucible in the places indicated by arrows in Figure 2. The melting/crystallization of etalons supposedly corresponded to the simultaneous phase transitions in Y_2O_3 loaded into the crucible. The growth rate was approximately 0.2–1 mm/h.

After cooling down the crucible to room temperature (Figure 3a), black ingots were extracted (Figure 3b). It was established that crystals grown for several hours were easily extracted from crucibles, whereas ingots grown for ≥ 24 h stuck to the crucible. In the latter case, ingots could not be extracted without destruction of the crucible.

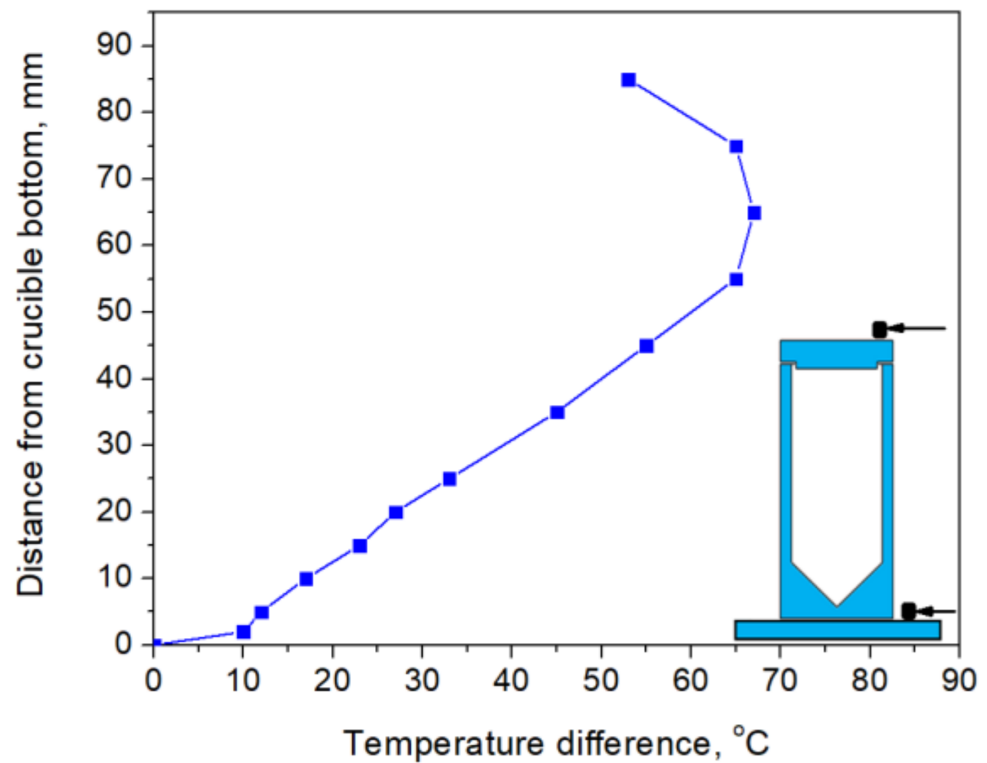


Figure 2. Axial temperature distribution in heat assembly without the crucible. The positions of Y_2O_3 etalons for controlling melting/crystallization inside the crucible are depicted by the arrows in the inset (the crucible drawing is presented for visualization purpose; its dimensions do not correspond to the temperature distribution).

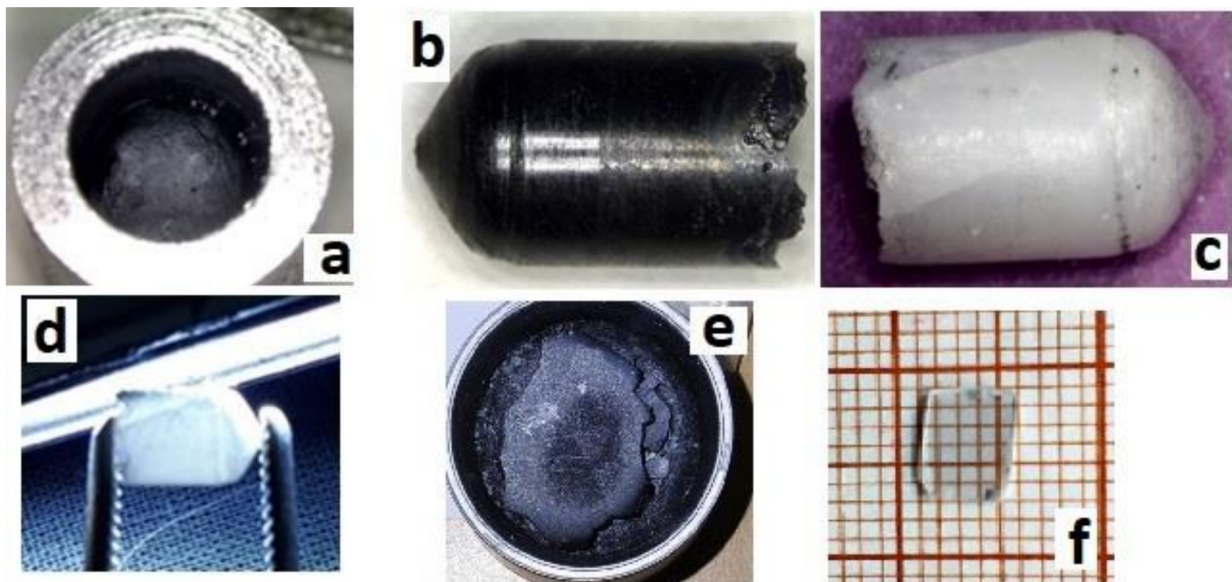


Figure 3. Obtained sesquioxide crystals: (a) Y_2O_3 with the diameter 6 mm as grown in crucible, (b) Y_2O_3 as grown extracted from the crucible, (c,d) Y_2O_3 after annealing in air at 1200 °C, (e) as-grown $Y_{1.1}Sc_{0.9}O_3$, and (f) polished sample with a thickness of 0.5 mm cut from the same $Y_{1.1}Sc_{0.9}O_3$ ingot after the annealing in air at 1200 °C.

Y_2O_3 crystals were annealed at 1200 °C for 12 h to reduce the number of defects caused by the growth in oxygen-deficient conditions. The annealed ingots were bleached

but translucent, with visible cracks (Figure 3c,d). Basically, the main obstacle in optimizing the crystal performance is the presence of polymorph transitions during the crystallization of Y_2O_3 from the melt. The cracks were eventually formed due to polymorphic phase transitions between H-, B (monoclinic), and C (cubic) phases occurring due to direct crystallization from the melt of Y_2O_3 and sesquioxides of lanthanides with ionic radii larger than approximately 0.085 nm [31]. This issue may be overcome by decreasing the average size of the rare earth cation in solid solutions of Y_2O_3 with Lu_2O_3 or Sc_2O_3 oxides, providing direct crystallization of the cubic phase from the melt. Analogous with [21], the mixed $Y_{1.1}Sc_{0.9}O_3$ oxide crystal was grown by the same procedure as described above for Y_2O_3 . The only difference was the sintering temperature, which was decreased to 2000 °C, because the melting temperature of the mixed composition is lower. The as-grown ingot was completely opaque (Figure 3e), however, the one annealed in air provided complete discoloration of the crystals. Transparent plates of $Y_{1.1}Sc_{0.9}O_3$ were obtained after cutting and polishing (Figure 3f). The crystal possesses a cubic structure (Sp.gr. $Ia-3$, $a = 10.2766 \text{ \AA}$). The lattice parameter of $Y_{1.11}Sc_{0.9}O_3$ (Figure 4a) is larger than 10.240 Å in the $YScO_3$ reference (Figure 4b) due to the higher content of yttrium. We evaluated the composition of this crystal assuming linearity between the lattice parameters and Y/Sc ratio. The calculated composition is $Y_{1.1}Sc_{0.9}O_3$, which completely corresponds to the melt composition, so there is no remarkable segregation of cations during the crystallization of this solid solution.

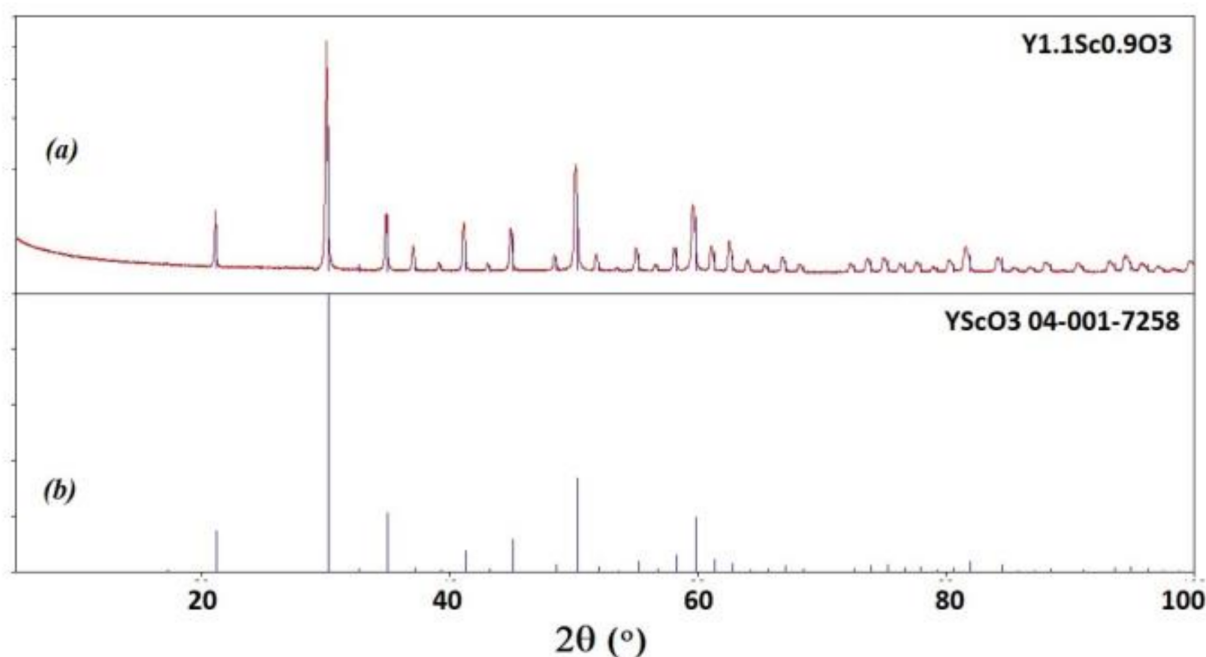


Figure 4. Powder diffraction patterns of $Y_{1.1}Sc_{0.9}O_3$ (a) in comparison with PDF 04-001-7258 $YScO_3$ reference (b).

3.3. Optical and Scintillation Characterization

Optical transmission of translucent Y_2O_3 could not be measured using the standard spectrometer at our disposal. Meanwhile, $Y_{1.1}Sc_{0.9}O_3$ mixed crystals (Figure 5) were transparent in the 230–1100 nm range, without any notable absorption peaks. The fundamental absorption edge at <230 nm corresponded to the literature values [32] of the band gap in sesquioxides of around 5–6 eV. The X-ray emission spectrum of the Y_2O_3 crystal (Figure 6a) had a weak intensity and contained a wide complex band in the 300–500 nm range with resolved sub-bands that peaked around 367, 417, and 486 nm and separate bands that peaked at 566 nm. The CL spectrum of this crystal possesses much stronger intensity

(Figure 6b) and contains two dominant bands that peaked at 444 and 495 nm, with a bump around 370 nm and a narrow peak at 572 nm.

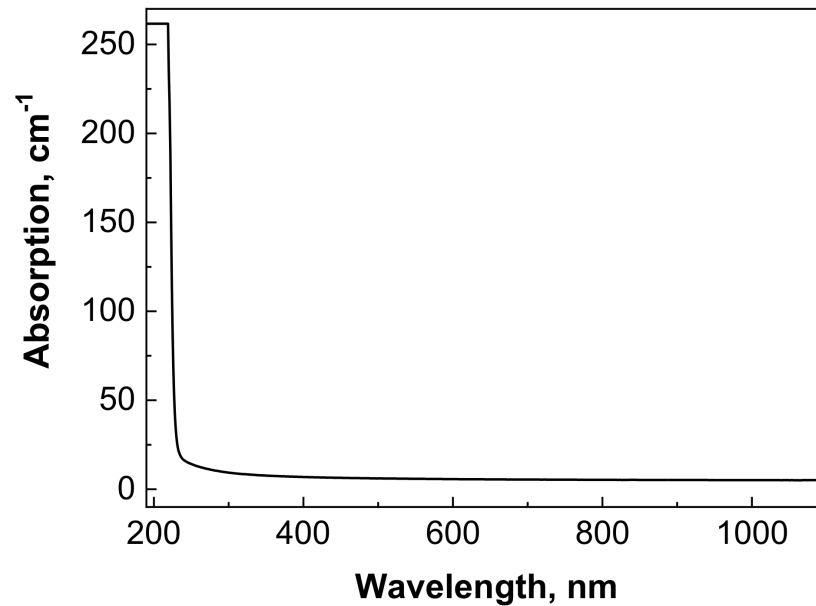


Figure 5. Optical absorption spectrum of $Y_{1.1}Sc_{0.9}O_3$ sample with a thickness of 0.5 mm.

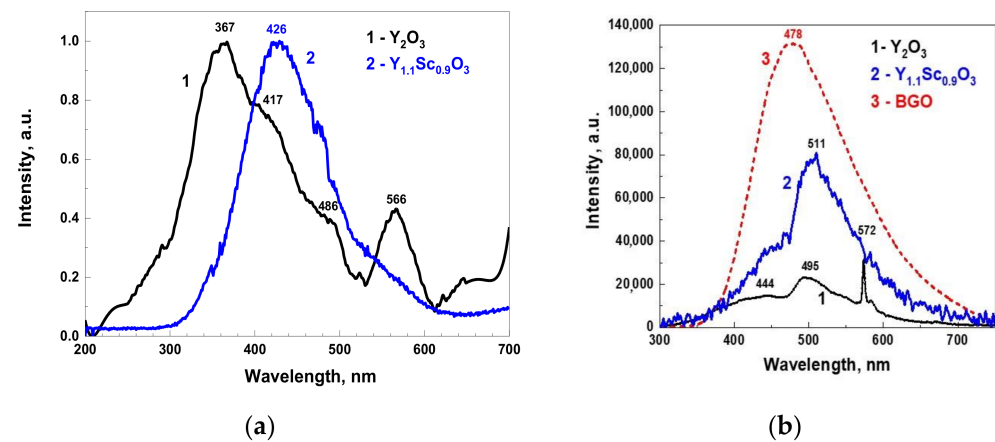


Figure 6. Normalized X-ray luminescence spectra of Y_2O_3 and $Y_{1.1}Sc_{0.9}O_3$ (a); cathodoluminescence spectra (b) of Y_2O_3 and $Y_{1.1}Sc_{0.9}O_3$ in comparison with the BGO reference crystal.

As the Y_2O_3 crystals in our experiments were grown in oxygen-poor conditions, the nature of the observed wide bands is probably associated with charged oxygen vacancies and their aggregates [33–37]. The nature of emission centers in Y_2O_3 crystals may be analyzed by comparing the XRL and CL spectra (Figure 6). The band that peaked around 370 nm dominates in the XRL spectra, while the CL spectrum consists of two broad emissions centered around 444 and 495 nm. Most likely, the mentioned bands are connected with the luminescence of F^+ and F centers and their aggregates with other defects of Y_2O_3 crystals [35–37]. We assumed that CL and XRL emission spectra also contain the components related to Cr^{3+} and Mn^{4+} trace impurities, because such dopants are typically presented in Y_2O_3 raw materials with 4N–5N purity.

However, it is important to note that the CL spectrum is much more intense in the visible range as compared to that observed under X-rays, as well as that reported in other publications [2,38]. This can be due to the quite different excitation conditions

(much stronger in the CL) and the different shaping time of the luminescence registration at respective setups (μs in XRL and ms in CL), as well as a deviation in the spectral sensitivities of experimental setups used for measurements of X-ray excited emission and cathodoluminescence spectra.

The light yield of Y_2O_3 was evaluated by comparing the squares under its CL spectrum with that of a standard BGO crystal taken in the same experimental conditions (Figure 6b). Assuming a BGO light yield as 8600 phot/MeV [28], the area under the Y_2O_3 peak is 19.5% of BGO, i.e., around 1700 phot/MeV. The X-ray luminescence spectrum of $\text{Y}_{1.1}\text{Sc}_{0.9}\text{O}_3$ (Figure 6c) was more intense as compared to that in Y_2O_3 and was represented by a wide band from 300 to 600 nm that peaked at 440 nm with a shoulder at 570 nm. The spectral band was remarkably red-shifted as compared to the Y_2O_3 XRL spectrum. The CL intensity of $\text{Y}_{1.1}\text{Sc}_{0.9}\text{O}_3$ was approximately 61.3% of BGO, corresponding to a light yield of approximately 5300 phot/MeV. The values for the mixed crystal are approximately in the middle between the light yield of 11,500–16,200 phot/MeV for Sc_2O_3 and 2600–3200 phot/MeV for Y_2O_3 , if assuming a monotonous increase in light yield from Y_2O_3 to Sc_2O_3 . Comparing the light yield with decay curves and luminescence spectra, one may link the increase in light yield with the slower emission of long-wavelength spectral components.

The scintillation decay curves of Y_2O_3 were fitted well ($R^2 > 0.998$) by single exponential decay functions, and the registered scintillation decay times were 33.2, 42.7, and 42.0 ns at excitation by α - and β -particles and γ -rays, respectively (Figure 7a). Such decay times are typical for the scintillation of Y_2O_3 ; for instance, the decay time of 34 ns under γ -rays was reported in [1] for ceramics. The nature of the differences in decay times under different types of excitations is a topic for a separate work. Here, we may just note that similar behavior (faster decay under α -particles and nearly similar kinetics under β -particles and γ -rays) was registered in garnet film scintillators (see for example [39,40]). The scintillation decay in the mixed $\text{Y}_{1.1}\text{Sc}_{0.9}\text{O}_3$ crystal at excitation by γ -rays was fitted rather well ($R^2 = 0.988$) by a two-exponential function with the decay constants of 36.7 and 403.2 ns (Figure 7b) with the contributions of 10.8 and 89.2%, respectively, to the overall signal. The decay constant of the fast component is similar to that in Y_2O_3 (42 ns), whereas the slow component may be tentatively attributed to Sc-related defects.

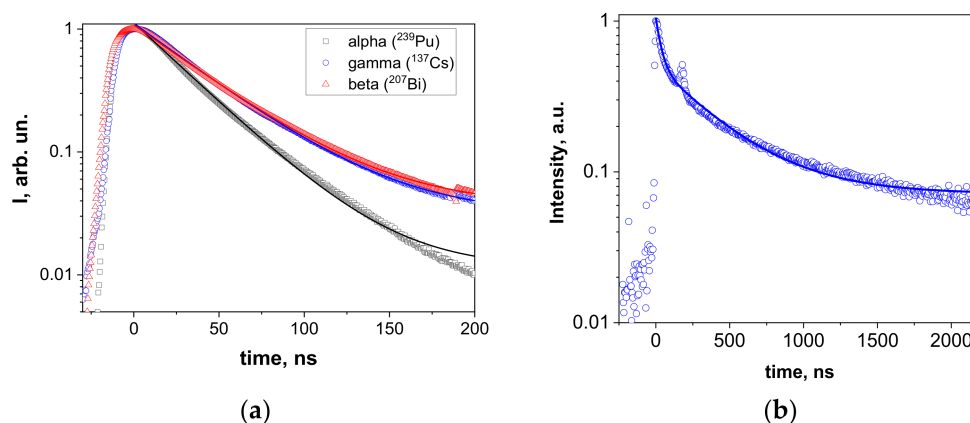


Figure 7. Scintillation decay in Y_2O_3 (a) at excitations with α - and β -particles and γ -rays and $\text{Y}_{1.1}\text{Sc}_{0.9}\text{O}_3$ (b) at excitation with γ -rays. The splash around 180 ns in (b) is an experimental artefact.

4. Conclusions

Y_2O_3 and $\text{Y}_{1.1}\text{Sc}_{0.9}\text{O}_3$ crystals were obtained for the first time by the VGF method in tungsten crucibles. The conducted experiments demonstrated that melt carbidization and polymorph transitions are the main obstacles for obtaining high-quality crystals. Carbidization may be effectively reduced by sealing the melt in the crucible from the CO-containing atmosphere by tungsten lid and screens, diminishing interactions between CO gas and Y_2O_3 melt. While Y_2O_3 crystals were translucent and contained numerous cracks due to

the polymorph transitions during the crystallization from the melt, transparent $Y_{1.1}Sc_{0.9}O_3$ crystals with crack-free parts were successfully obtained. The issue of polymorph transitions was resolved by decreasing the average radius of the rare earth cation by switching to Sc_2O_3 – Y_2O_3 solid solutions.

Luminescent and scintillation parameters of the obtained crystals were studied. Typical luminescence bands attributed to defects in Y_2O_3 were registered, as well as luminescence decay times of 33–43 ns depending on the type of ionizing radiation. The light yield of cathodoluminescence was around 1700 phot/MeV. $Y_{1.1}Sc_{0.9}O_3$ are transparent from 230 nm, possess more intense luminescence with a light yield of approximately 5300 phot/MeV, and the second slow decay component of ~400 ns, which may be tentatively attributed to Sc-related defects.

The obtained results demonstrate the reliability of the VGF method and W crucibles for the growth of single crystals of lanthanides, yttrium, and scandium sesquioxides. Furthermore, they open a perspective of obtaining these sesquioxides in W crucibles by Bridgman and Czochralski methods, although the problem of melt insulation from the growth atmosphere may be critical for the Czochralski growth process.

Author Contributions: Investigation, V.G., D.K., S.T., P.A., S.S., V.A., A.S., I.B. and V.N.; data curation, I.G.; writing—original draft preparation, E.G. and S.W.-L.; measurements, data curation, editing, writing—review and editing, Y.Z.; writing—review and editing, O.S. All authors have read and agreed to the published version of the manuscript.

Funding: This work was carried out in the frame of the National Academy of Science of Ukraine Projects KORZE (reg. no. 0121U108986), “Carbon-2” (reg. no. 0122U002637). S.S. and O.S. acknowledge the support from the “ENSEMBLE3” project (GA no. MAB/2020/14) carried out within the International Research Agendas program of the Foundation for Polish Science and Teaming for Excellence project (GA no. 857543). S.W.L. and Y.Z. also acknowledge the support from the Polish NCN UMO-2018/31/B/ST8/03390 project.

Data Availability Statement: Not applicable.

Conflicts of Interest: The authors declare no conflict of interest. The funders had no role in the design of the study; in the collection, analyses, or interpretation of data; in the writing of the manuscript; or in the decision to publish the results.

References

1. Futami, Y.; Yanagida, T.; Fujimoto, Y.; Pejchal, J.; Sugiyama, M.; Kurosawa, S.; Yokota, Y.; Ito, A.; Yoshikawa, A.; Goto, T. Optical and scintillation properties of Sc_2O_3 , Y_2O_3 and Lu_2O_3 transparent ceramics synthesized by SPS method. *Radiat. Meas.* **2013**, *55*, 136–140. [[CrossRef](#)]
2. Fukabori, A.; Chani, V.; Kamada, K.; Moretti F.; Yoshikawa, A. Growth of Tm^{3+} -doped Y_2O_3 , Sc_2O_3 , and Lu_2O_3 crystals by the micropulling down technique and their optical and scintillation characteristics. *Cryst. Growth Des.* **2011**, *11*, 2404–2411. [[CrossRef](#)]
3. Thoř, T.; Rubeřova, K.; Jakeř, V.; Cajzl, J.; Nadherny, L.; Mikolařova, D.; Kučerkova, R.; Nikl, M. Lanthanide-doped Lu_2O_3 phosphors and scintillators with green-to-red emission. *J. Lumin.* **2019**, *215*, 116647. [[CrossRef](#)]
4. Thoř, T.; Rubeřova, K.; Jakeř, V.; Cajzl, J.; Nadherny, L.; Mikolařova, D.; Beitlerova, A.; Nikl, M. Europium-doped Lu_2O_3 phosphors prepared by a sol-gel method. *IOP Conf. Ser. Mater. Sci. Eng.* **2018**, *465*, 012009. [[CrossRef](#)]
5. Pirri, A.; Toci, G.; Patrizi, B.; Vannini, M. An overview on Yb-Doped transparent polycrystalline sesquioxide laser ceramics. *IEEE J. Sel. Top. Quantum Electron.* **2018**, *24*, 1–8. [[CrossRef](#)]
6. Liu, Z.; Toci, G.; Pirri, A.; Patrizi, B.; Feng, Y.; Chen, X.; Hu, D.; Feng, T.; Lexiang, W.; Matteo, V.; et al. Fabrication and Optical Property of Nd:Lu₂O₃ Transparent Ceramics for Solid-state Laser Applications. *Inorg. Mater.* **2020**, *36*, 210–216. [[CrossRef](#)]
7. Hlavac, J. Melting temperatures of refractory oxides: Part I. *Pure Appl. Chem.* **1982**, *54*, 681–688. [[CrossRef](#)]
8. Coutures, J.P.; Rand, M.H. Melting temperatures of refractory oxides-Part II: Lanthanoid sesquioxides. *Pure Appl. Chem.* **1989**, *61*, 1461–1482. [[CrossRef](#)]
9. Zhang, J.; Chen, H.; Wang, J.; Wang, D.; Han, D.; Zhang, J.; Wang, S. Preparation of $(Tb_{1-x}Lu_x)_2O_3$ transparent ceramics by solid solution for magneto-optical application. *J. Eur. Ceram. Soc.* **2021**, *41*, 2818–2825. [[CrossRef](#)]
10. Südmeyer, T.; Krankel, C.; Baer, C.R.E.; Heckl, O.H.; Saraceno, C.J.; Golling, M.; Peters, R.; Petermann, K.; Huber, G.; Keller, U. High-power ultrafast thin disk laser oscillators and their potential for sub-100-femtosecond pulse generation. *Appl. Phys. B* **2009**, *97*, 281–295. [[CrossRef](#)]
11. Krankel, C. Rare-earth-doped sesquioxides for diode-pumped high-power lasers in the 1-, 2-, and 3- μ m spectral range. *IEEE J. Sel. Top. Quantum. Electron.* **2014**, *21*, 250–262. [[CrossRef](#)]

12. Boulesteix, R.; Epherre, R.; Noyau, S.; Vandenhende, M.; Maitre, A.; Sallé, C.; Alombert-Goget, G.; Guyot, Y.; Brenier, A. Highly transparent Nd: Lu₂O₃ ceramics obtained by coupling slip-casting and spark plasma sintering. *Scr. Mater.* **2014**, *75*, 54–57. [[CrossRef](#)]
13. Kryzhanovska, O.S.; Baumer, V.N.; Parkhomenko, S.V.; Doroshenko, A.G.; Yavetskiy, R.P.; Balabanov, A.E.; Tolmachev, A.V.; Skorik, S.N.; Li, J.; Kuncser, A. Formation peculiarities and optical properties of highly-doped (Y_{0.86}La_{0.09}Yb_{0.05})₂O₃ transparent ceramics. *Ceram. Int.* **2019**, *45*, 16002–16007. [[CrossRef](#)]
14. Kim, K.J.; Kamada, K.; Murakami, R.; Horiai, T.; Ishikawa, S.; Kochurikhin, V.V.; Yoshino, M.; Yamaji, A.; Shoji, Y.; Kurosawa, S.; et al. Growth of Lu₂O₃ and HfO₂ Based High Melting Temperature Single Crystals by Indirect Heating Method Using Arc Plasma. *Crystals* **2020**, *10*, 619. [[CrossRef](#)]
15. Zhang, N.; Yin, Y.; Zhang, J.; Wang, T.; Wang, S.; Yin, Y.; Fu, X.; Jia, Z.; Tao, X. Optimized growth of high length-to-diameter ratio Lu₂O₃ single crystal fibers by the LHPG method. *CrystEngComm* **2021**, *23*, 1657–1662. [[CrossRef](#)]
16. Hou, W.; Zhao, H.; Li, N.; Xue, Y.; Shi, J.; Xu, X.; Xu, J. Growth and spectroscopic properties of Er: Lu₂O₃ crystal grown by floating zone method. *Mater. Res. Express* **2019**, *6*, 066203. [[CrossRef](#)]
17. Guzik, M.; Pejchal, J.; Yoshikawa, A.; Ito, A.; Goto, T.; Siczek, M.; Lis, T.; Boulon, G. Structural investigations of Lu₂O₃ as single crystal and polycrystalline transparent ceramic. *Cryst. Growth Des.* **2014**, *14*, 3327–3334. [[CrossRef](#)]
18. Yin, Y.; Wang, G.; Jia, Z.; Mu, W.; Fu, X.; Zhang, J.; Tao, X. Controllable and directional growth of Er: Lu₂O₃ single crystals by the edge-defined film-fed technique. *CrystEngComm* **2020**, *22*, 6569–6573. [[CrossRef](#)]
19. Peters, R.; Kränkel, C.; Petermann, K.; Huber, G. Crystal growth by the heat exchanger method, spectroscopic characterization and laser operation of high-purity Yb:Lu₂O₃. *J. Cryst. Growth* **2008**, *310*, 1934–1938. [[CrossRef](#)]
20. Hu, K.; Zheng, L.; Zhang, H. Control of interface shape during high melting sesquioxide crystal growth by HEM technique. *J. Cryst. Growth* **2018**, *483*, 175–182. [[CrossRef](#)]
21. Kränkel, C.; Uvarova, A.; Haurat, É.; Hülshoff, L.; Brützmam, M.; Guguschev, C.; Kalusniak, S.; Klimm, D. Czochralski growth of mixed cubic sesquioxide crystals in the ternary system Lu₂O₃–Sc₂O₃–Y₂O₃. *Acta. Crystallogr. B. Struct. Sci. Cryst. Eng. Mater.* **2021**, *77*, 550–558. [[CrossRef](#)]
22. Suzuki, A.; Kalusniak, S.; Tanaka, H.; Brützmam, M.; Ganschow, S.; Tokurakawa, M.; Kränkel, C. Spectroscopy and 2.1 μm laser operation of Czochralski-grown Tm³⁺:YScO₃ crystals. *Opt. Express* **2022**, *30*, 42762–42771. [[CrossRef](#)] [[PubMed](#)]
23. Dong, J.; Zhao, H.; Cao, X.; Wang, W.; Xu, X.; Wu, F.; Luo, P.; Wang, Q.; Xue, Y.; Xu, J. Crystal growth and spectroscopic analysis of Ho, Pr:Sc₂O₃ crystal for 2.9 μm mid-IR laser. *Opt. Mater. Express* **2021**, *11*, 2539–2546. [[CrossRef](#)]
24. Sidletskiy, O.; Gerasymov, I.; Boyaryntseva, Y.; Arhipov, P.; Tkachenko, S.; Zelenskaya, O.; Bryleva, K.; Belikov, K.; Lebbou, K.; Dujardin, C.; et al. Impact of Carbon Co-Doping on the Optical and Scintillation Properties of a YAG: Ce Scintillator. *Cryst. Growth Des.* **2021**, *21*, 3063–3070. [[CrossRef](#)]
25. Tkachenko, S.; Arhipov, P.; Gerasymov, I.; Galenin, E.; Shaposhnyk, A.; Hryshyna, O.; Mateychenko, P.; Boyaryntseva, Y.; Zelenskaya, O.; Lebbou, K.; et al. The crystal growth of ortho- and pyrosilicates from W and Mo crucibles. *CrystEngComm* **2021**, *23*, 360–367. [[CrossRef](#)]
26. Gerasymov, I.; Hubenko, K.; Viagin, O.; Boyaryntseva, Y.; Shaposhnyk, A.; Baumer, V.; Gorbacheva, T.; Zelenskaya, O.; Galenin, E.; Kurtsev, D.; et al. Characterization of LaGPS:Ce scintillation crystals obtained under a reducing atmosphere. *CrystEngComm* **2022**, *24*, 7066–7072. [[CrossRef](#)]
27. Scintillation Properties—Lawrence Berkeley National Laboratory. Available online: [Scintillator.lbl.gov](https://scintillator.lbl.gov) (accessed on 13 March 2023).
28. Sidletskiy, O.; Arhipov, P.; Tkachenko, S.; Zelenskaya, O.; Vasyukov, S.; Moretti, F.; Dujardin, C. Drastic Scintillation Yield Enhancement of YAG:Ce with Carbon Doping. *Phys. Status Solidi A* **2018**, *215*, 1800122. [[CrossRef](#)]
29. Holleman, A.F.; Wiberg, E.; Wiberg, N. *Inorganic Chemistry*; Academic Press: Cambridge, MA, USA, 2001.
30. Nizhankovsky, S.; Krivososov, E.; Baranov, V.; Budnikov, A.; Kanishchev, V.; Grin, L.; Adonkin, G. Optical homogeneity of Ti:sapphire crystals grown by horizontal directional solidification. *Inorg. Mater.* **2012**, *48*, 1111–1114. [[CrossRef](#)]
31. Adachi, G.; Imanaka, N. The binary rare earth oxides. *Chem. Rev.* **1998**, *98*, 1479–1514. [[CrossRef](#)]
32. Badehian, H.A.; Salehi, H.; Ghoohestani, M. First-principles study of elastic, structural, electronic, thermodynamical, and optical properties of Yttria (Y₂O₃) ceramic in cubic phase. *J. Am. Ceram. Soc.* **2013**, *96*, 1832–1840. [[CrossRef](#)]
33. Lushchik, A.; Kirm, M.; Lushchik Ch Martinson, I.; Zimmerer, G. Luminescence of free and self-trapped excitons in wide-gap oxides. *J. Lumin.* **2000**, *87–89*, 232–234. [[CrossRef](#)]
34. Zheng, J.X.; Ceder, G.; Maxisch, T.; Chim, W.K.; Choi, W.K. Native point defects in yttria and relevance to its use as a high-dielectric-constant gate oxide material: First-principles study. *Phys. Rev. B* **2006**, *73*, 104101. [[CrossRef](#)]
35. Nambu, K.; Hayasaka, H.; Yamamoto, T.; Yoshida, H. Photoluminescence properties of undoped and Si⁴⁺-doped polycrystalline Y₂O₃ phosphors prepared by flash-sintering. *Appl. Phys. Express* **2019**, *12*, 075504. [[CrossRef](#)]
36. Huang, H.; Sun, X.; Wang, S.; Liu, Y.; Li, X.; Liu, J.; Kang, Z.; Lee, S.-T. Strong red emission of pure Y₂O₃ nanoparticles from oxygen related defects. *Dalton Trans.* **2011**, *40*, 11362–11366. [[CrossRef](#)]
37. Zorenko, Y.; Zorenko, T.; Voznyak, T.; Mandowski, A.; Xia, Q.; Batentschuk, M.; Fridrich, J. Luminescence of F⁺ and F centers in Al₂O₃-Y₂O₃ oxide compounds. *IOP Conf. Ser. Mater. Sci. Eng.* **2010**, *15*, 012060. [[CrossRef](#)]
38. Kumar, Y.; Pal, M.; Herrera, M.; Mathew, X. Effect of Eu ion incorporation on the emission behavior of Y₂O₃ nanophosphors: A detailed study of structural and optical properties. *Opt. Mater.* **2016**, *60*, 159–168. [[CrossRef](#)]

39. Witkiewicz-Lukaszek, S.; Gorbenko, V.; Zorenko, T.; Syrotych, Y.; Mares, J.A.; Nikl, M.; Sidletskiy, O.; Bilski, P.; Yoshikawa, A.; Zorenko, Y. Composite Detectors Based on Single-Crystalline Films and Single Crystals of Garnet Compounds. *Materials* **2022**, *15*, 1249. [[CrossRef](#)]
40. Sidletskiy, O.; Gorbenko, V.; Zorenko, T.; Syrotych, Y.; Witkiewicz-Lukaszek, S.; Mares, J.A.; Kucerkova, R.; Nikl, M.; Gerasymov, I.; Kurtsev, D.; et al. Composition Engineering of $(\text{Lu,Gd,Tb})_3(\text{Al,Ga})_5\text{O}_{12}:\text{Ce}$ Film/ $\text{Gd}_3(\text{Al,Ga})_5\text{O}_{12}:\text{Ce}$ Substrate Scintillators. *Crystals* **2022**, *12*, 1366. [[CrossRef](#)]

Disclaimer/Publisher's Note: The statements, opinions and data contained in all publications are solely those of the individual author(s) and contributor(s) and not of MDPI and/or the editor(s). MDPI and/or the editor(s) disclaim responsibility for any injury to people or property resulting from any ideas, methods, instructions or products referred to in the content.